LA-UR- 98-4071

*Approved for public release; distribution is unlimited.*

Title: ADAPTIVE FEEDFORWARD OF ESTIMATED RIPPLE IMPROVES THE CLOSE LOOP RF SYSTEM PERFORMANCE SIGNIFICANTLY

CONF-990602--



Author(s): S. Kwon, A. H. Regan, Y. M. Wang, A. S. Rohlev

Submitted to: American Control Conf., San Diego, CA, 6/2-4/99



**Los Alamos**
NATIONAL LABORATORY

Title: **ADAPTIVE FEEDFORWARD OF ESTIMATED RIPPLE IMPROVES THE CLOSED LOOP SYSTEM PERFORMANCE SIGNIFICANTLY**

**Authors: Sung-il Kwon, Amy Regan, Y. M. Wang, and T. Rohlev**
**RF Technology Group**
**Accelerator Operations and Technology Division**
**Los Alamos National Laboratory**
**E-mail: skwon@lanl.gov**

Submitted to: 1999 American Control Conference, San Diego, CA.

**Remark:** The second sections of the paper entitled "Adaptive feedforward ..." , the paper entitled "Phase synchronization ...", and the paper entitled "Feedback linearization ..." are describing the klystron model and are almost same. Also, the third sections of the paper entitled "Adaptive feedforward ..." and the paper entitled "Feedback linearization ..." are describing the RF cavity model and almost same. The rest sections of each paper describe the different control techniques and they are derived from the klystron model and the RF cavity model described in the second section and the third section. When at least two papers are accepted for full papers, the second section and the third section will be modified.

## DISCLAIMER

## DISCLAIMER

Portions of this document may be illegible in electronic image products. Images are produced from the best available original document.

# ADAPTIVE FEEDFORWARD OF ESTIMATED RIPPLE IMPROVES THE CLOSED LOOP SYSTEM PERFORMANCE SIGNIFICANTLY

Sung-il Kwon, Amy Regan, Y. M. Wang, and T. Rohlev
RF Technology Group
Accelerator Operations and Technology Division
Los Alamos National Laboratory
P.O.Box 1663
Los Alamos, NM 87544, USA
E-mail: skwon@lanl.gov

**Abstract**-The Low Energy Demonstration Accelerator(LEDA) being constructed at Los Alamos National Laboratory will serve as the prototype for the low energy section of Acceleration Production of Tritium(APT) accelerator. This paper addresses the problem of LLRF control system for LEDA. We propose an estimator of the ripple and its time derivative and a control law which is based on PID control and adaptive feedforward of estimated ripple. The control law reduces the effect of the deterministic cathode ripple that is due to high voltage power supply and achieves tracking of desired set points.

## 1 Introduction

The low energy demonstration accelerator(LEDA) for the Accelerator Production of Tritium(APT) is being built at Los Alamos National Laboratory. The primary function of the

low level RF(LLRF) control system of LEDA is to control RF fields in the accelerating cavity and maintain field stability within $\pm 1\%$ peak to peak amplitude error and $1^\circ$ peak to peak phase error[5].

This paper addresses the problem of LLRF control system attenuating the effect of ripple on the klystron cathode voltage that results from the high voltage power supply ripple. We propose a PID control law coupled with an adaptive feedforward of ripple estimate. The purpose of control is to reduce the effect of the deterministic cathode ripple that is due to harmonics of high voltage power supply[4] and is to achieve tracking of desired set points. Low frequency ripple does not deteriorate current LLRF control system performance based on current PID control methodology. As frequency of the ripple increases, however, the effect of the ripple on the performance increases too. Simulation shows that 0.3% high voltage power supply ripple yields $1.05^\circ$ peak to peak phase error at about $72kHz$ [3] and 1.0% high voltage power supply ripple yields $1.07^\circ$ peak to peak phase error at about $20kHz$[7]. In order to suppress the high frequency ripple effect, the proposed controller makes use of a feedforward control coupled with a ripple estimator. The high voltage power supply ripple is coupled to the LEDA through a klystron. The effects of the ripple are on both the amplitude and the phase of a klystron. In [6],[7], the influences of the ripple are modeled by algebraic equations. A klystron is modeled by a nonlinear state space system[6],[7]. We, first, address two coordinate transformations of a klystron model. Based on new coordinates, we extract the ripple equation which is represented by algebraic equations of states of new coordinates. The ripple estimator proposed in this work is based on the algebraic equation and it estimates the ripple signal itself and the time derivative of the ripple as well. The estimate of ripple is feedforwarded to the current LLRF control system whose frame is a PID control. This simple addition of an adaptive feedforward greatly improves the closed loop system performance.

# 2 The Klystron Model

We consider a klystron model as shown in as shown in Figure 1.

It has two inputs, LLRF_I and LLRF_Q and two output HPRF_I and HPRF_Q. As intermediate outputs, Klystron has the normalized amplitude **N_AMPLITUDE** and the normalized phase **N_PHASE**.

The first stage of a klystron are linear systems called **FILTER AND AMPLIFIER**. Let $u_1$=LLRF_I and let $u_2$=LLRF_Q. Let $x_1$ and $x_2$ be outputs of the systems whose transfer

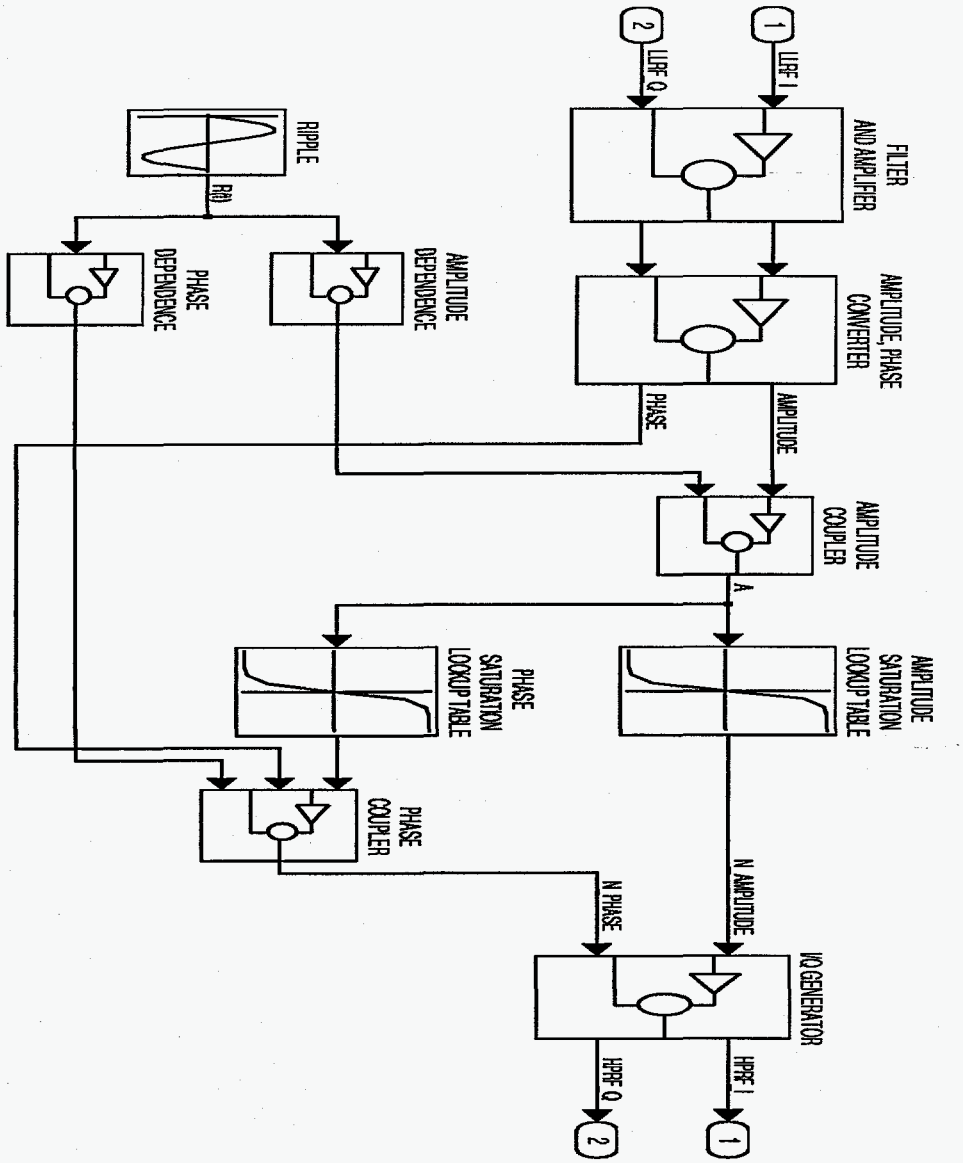


Figure 1: A Klystron Model

function are given by

$$\frac{X_1(s)}{U_1(s)} = \frac{1}{3.54e^{-7}s + 1} \tag{1}$$

$$\frac{X_2(s)}{U_2(s)} = \frac{1}{3.54e^{-7}s + 1}. \tag{2}$$

In state space, transfer functions (1) and (2) are represented as

$$\dot{x}_1 = -a_1 x_1 + a_1 u_1 \tag{3}$$

$$\dot{x}_2 = -a_1 x_2 + a_1 u_2 \tag{4}$$

where $a_1 = \frac{1e^{+007}}{3.54}$.

A klystron model has two loop-up tables, called **AMPLITUDE SATURATION** and **PHASE SATURATION**. The input of the two look-up tables is given by

$$A = \frac{K_g}{10\sqrt{KP_m}}(0.01R(t) + 1)^{1.25} \cdot \sqrt{x_1^2 + x_2^2} \tag{5}$$

where $R(t)$ is the ripple, $K_g$ is the klystron gain, and $KP_m$ is the maximum klystron power. $R(t)$, $K_g$, and $KP_m$ are specified for a given klystron. For given A, the output of the look-up table **AMPLITUDE SATURATION** can be represented by

$$A_N = I_1(A) \tag{6}$$

and the output of the look-up table **PHASE SATURATION** can be represented by

$$\theta_N = I_2(A) \tag{7}$$

Table 1 and table 2 show data of look-up table **AMPLITUDE SATURATION** and data of look-up table **PHASE SATURATION**, respectively.

The normalized amplitude N_Amplitude, defined by $y_1^k$ and the normalized phase N_Phase, defined by $y_2^k$ of the klystron are expressed by

$$y_1^k = A_N = I_1(A) \tag{8}$$

$$\begin{aligned} y_2^k &= \theta_N + tan^{-1}(\frac{x_2}{x_1}) + 3 \cdot \frac{\pi}{180} \cdot R(t) \\ &= I_2(A) + tan^{-1}(\frac{x_2}{x_1}) + 3 \cdot \frac{\pi}{180} \cdot R(t). \end{aligned} \tag{9}$$

In addition, for given $y_1$ and $y_2$, HPRF_I and HPRF_Q are given by

$$HPRF\_I = 10\sqrt{KP_m} \cdot y_1^k \cdot cos(y_2^k) \tag{10}$$

$$HPRF\_Q = 10\sqrt{KP_m} \cdot y_1^k \cdot sin(y_2^k). \tag{11}$$

| $A$ | $A_N$ | $A$ | $A_N$ | $A$ | $A_N$ | $A$ | $A_N$ |
|---|---|---|---|---|---|---|---|
| -0.1000 | 0.0000 | 0.0700 | 0.0000 | 0.1400 | 0.1900 | 0.5700 | 0.7500 |
| 0.7100 | 0.8700 | 0.8600 | 0.9800 | 0.9000 | 1.0000 | 0.9100 | 1.0000 |
| 0.3122 | 0.4143 | 0.3568 | 0.4724 | 0.4014 | 0.5305 | 0.4461 | 0.5886 |
| 0.4907 | 0.6467 | 0.5353 | 0.7048 | 0.5799 | 0.7585 | 0.5910 | 0.7680 |
| 1.0000 | 0.9900 | 0.4461 | 0.5886 | 0.6468 | 0.8158 | 0.6691 | 0.8349 |
| 0.0446 | 0.0000 | 0.0892 | 0.0521 | 0.6914 | 0.8540 | 0.7360 | 0.8891 |
| 0.1338 | 0.1732 | 0.1784 | 0.2400 | 0.7806 | 0.9218 | 0.8252 | 0.9545 |
| 0.2230 | 0.2981 | 0.2676 | 0.3562 | 0.8921 | 0.9961 | 0.9367 | 0.9970 |
| 0.3122 | 0.4143 | 0.3568 | 0.4724 | 0.9813 | 0.9921 | | |

Table 1. AMPLITUDE SATURATION Data

| $A$ | $\theta_N$ | $A$ | $\theta_N$ | $A$ | $\theta_N$ | $A$ | $\theta_N$ |
|---|---|---|---|---|---|---|---|
| -0.1000 | 0.0000 | 0.0700 | 0.0000 | 0.6400 | -0.0150 | 0.7100 | -0.0350 |
| 0.8600 | -0.1370 | 0.9000 | -0.2440 | 1.0000 | -0.4770 | 0.0446 | 0.0000 |
| 0.4987 | -0.0113 | 0.5445 | -0.0125 | 0.5576 | -0.0128 | 0.6691 | -0.0233 |
| 0.0892 | -5.0552e-4 | 0.1338 | -0.0017 | 0.5712 | -0.0132 | 0.7140 | -0.0377 |
| 0.1784 | -0.0029 | 0.2230 | -0.0040 | 0.8921 | -0.2229 | 0.4549 | -0.0101 |
| 0.2676 | -0.0052 | 0.3122 | -0.0064 | 0.4483 | -0.0100 | 0.4014 | -0.0087 |
| 0.3568 | -0.0075 | 0.7885 | -0.0884 | 0.9593 | -0.3821 | | |

Table 2. PHASE SATURATION Data

Since the look-up tables have the limited number of data, we need to approximate the look-up tables by linear or nonlinear curve fitting equations. Considering the characteristic curve of a klystron, we choose nonlinear equations. We choose curve fitting equations of **AMPLITUDE SATURATION** and **PHASE SATURATION** having the forms

$$A_N = \sum_{i=1}^{N} c_i e^{-f_i A} \tag{12}$$

$$\theta_N = \sum_{i=1}^{N} d_i e^{-f_i A} \tag{13}$$

where $f_i$, $i = 1, 2, \cdots, N$ and parameters $c_i$, $i = 1, 2, \cdots, N$, $d_i$, $i = 1, 2, \cdots, N$ are to be determined.

Higher order of a curve fitting equation may yield more accurate curve fitting equation. For simplicity, we choose $N = 7$. Also, in order to reduce the number of coefficients to be determined, $f_i$, $i = 1, 2, \cdots, N$ are given in Table 3.

| $f_1$ | $f_2$ | $f_3$ | $f_4$ | $f_5$ | $f_6$ | $f_7$ |
|---|---|---|---|---|---|---|
| 0.50 | 0.75 | 1.00 | 1.25 | 1.50 | 1.75 | 2.00 |

Table 3. Exponents of curve fitting equations

By using data given in Table 1 and Table 2, we obtain coefficients $c_i$, $i = 1, 2, \cdots, N$ and $d_i$, $i = 1, 2, \cdots, N$, of the curve fitting equations (12) and (13). Coefficients $c_i$ and $d_i$ obtained are given in Table 4. Figure 2 shows plots of data points as given in Table 4, Table 5 and plots of curve fitting equations (12) and (13) whose coefficients, $f_i$, $i = 1, 2, \cdots, N$, $c_i$, $i = 1, 2, \cdots, N$, $d_i$, $i = 1, 2, \cdots, N$, are given in Table 3 and Table 4 with appropriate domain of $A$.

| | | | |
|---|---|---|---|
| $c_1$ | 0.05680429876058e+006 | $d_1$ | -0.14120739315590e+005 |
| $c_2$ | -0.39264357353961e+006 | $d_2$ | 0.83084262097993e+005 |
| $c_3$ | 1.12805594234952e+006 | $d_3$ | -2.01778226478032e+005 |
| $c_4$ | -1.72418545240933e+006 | $d_4$ | 2.58441412755651e+005 |
| $c_5$ | 1.47878241712872e+006 | $d_5$ | -1.83680595711727e+005 |
| $c_6$ | -0.67483667002473e+006 | $d_6$ | 0.68453128529433e+005 |
| $c_7$ | 0.12802296547207e+006 | $d_7$ | -0.10399245992504e+005 |

Table 4. Coefficients of curve fitting equations

Plugging (5) to (12) and (13), curve fitting equations (12) and (13) are reduced to

$$A_N = \sum_{i=1}^{N} c_i e^{-f_i w(t)\sqrt{x_1^2+x_2^2}} \tag{14}$$

$$\theta_N = \sum_{i=1}^{N} d_i e^{-f_i w(t)\sqrt{x_1^2+x_2^2}} \tag{15}$$

where

$$w(t) = \frac{K_g}{10\sqrt{KP_m}}(0.01R(t)+1)^{1.25}. \tag{16}$$

The normalized amplitude $y_1^k$ and the normalized phase $y_2^k$ of the klystron are

$$\begin{aligned} y_1^k &= A_N = \sum_{i=1}^{N} c_i e^{-f_i w(t)\sqrt{x_1^2+x_2^2}} && (17)\\ y_2^k &= \theta_N + tan^{-1}(\frac{x_2}{x_1}) + 3\cdot\frac{\pi}{180}\cdot R(t) \\ &= \sum_{i=1}^{N} d_i e^{-f_i w(t)\sqrt{x_1^2+x_2^2}} + tan^{-1}(\frac{x_2}{x_1}) + 3\cdot\frac{\pi}{180}\cdot R(t). && (18) \end{aligned}$$

In addition, for given $y_1^k$ and $y_2^k$, HPRF_I and HPRF_Q are given by

$$HPRF\_I = 10\sqrt{KP_m}\cdot y_1^k \cdot cos(y_2^k) \tag{19}$$

$$HPRF\_Q = 10\sqrt{KP_m}\cdot y_1^k \cdot sin(y_2^k). \tag{20}$$

## 2.1 The Klystron in $z$-coordinate

Consider the normalized amplitude $y_1^k$ and the normalized phase $y_2^k$ as given in (17) and (18).

Let

$$z_1 = \sqrt{x_1^2+x_2^2} \tag{21}$$

$$z_2 = tan^{-1}(\frac{x_2}{x_1}). \tag{22}$$

We consider a transformation from $x$-coordinate to $z$-coordinate. In $z$-coordinate, the state equations (3) and (4) are reduced to

$$\dot{z}_1 = -a_1 z_1 + a_1 cos(z_2)u_1 + a_1 sin(z_2)u_2 \tag{23}$$

$$\dot{z}_2 = -a_1\frac{sin(z_2)}{z_1}u_1 + a_1\frac{cos(z_2)}{z_1}u_2. \tag{24}$$

Also, the curve fitting equations (12) and (13) are reduced to

$$A_N = \sum_{i=1}^{N} c_i e^{-f_i w(t) z_1} \tag{25}$$

$$\theta_N = \sum_{i=1}^{N} d_i e^{-f_i w(t) z_1}. \tag{26}$$

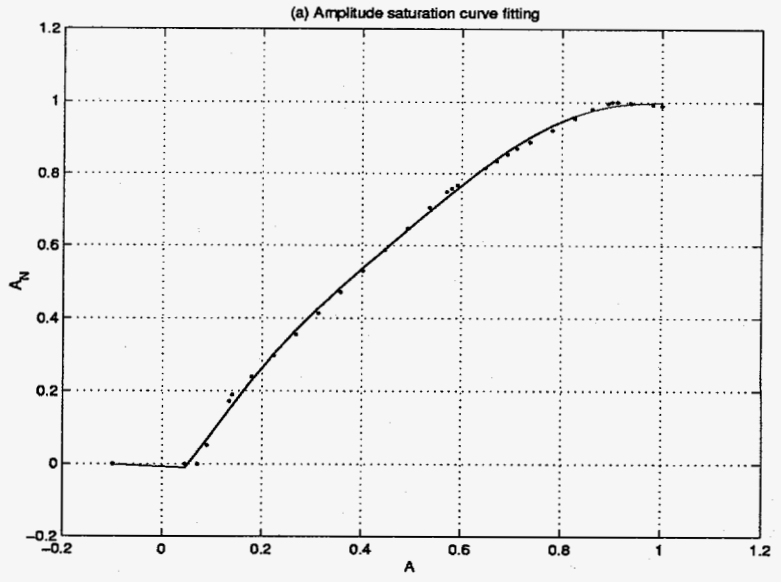


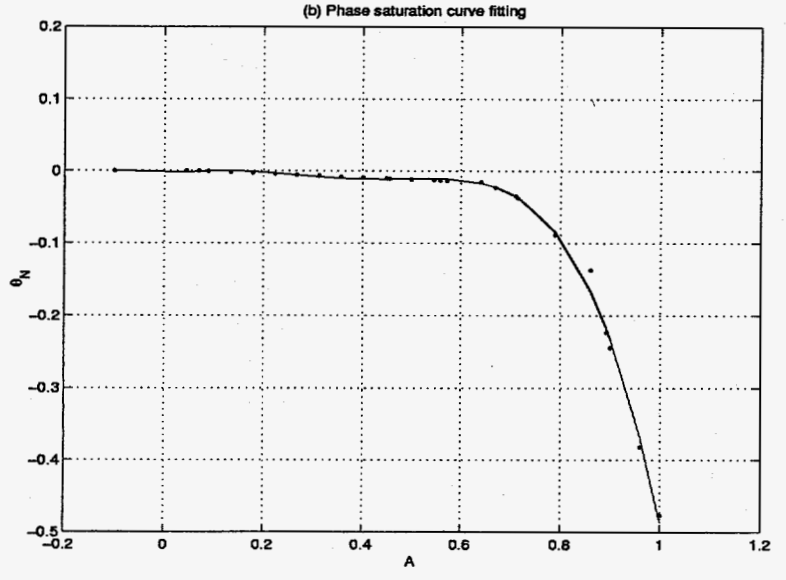


Figure 2: Curve fittings

The normalized amplitude $y_1^k$ and the normalized phase $y_2^k$ are represented by

$$y_1^k = \sum_{i=1}^{N} c_i e^{-f_i w(t) z_1} \tag{27}$$

$$y_2^k = \sum_{i=1}^{N} d_i e^{-f_i w(t) z_1} + z_2 + 3 \cdot \frac{\pi}{180} \cdot R(t). \tag{28}$$

Note that the exponents of the first term of (27) are the same as the exponents of the first term of (28). Also, note that the phase $y_2^k$ is linear with respect to $z_2$.

## 2.2 The Klystron in $\overline{z}$-coordinate

Consider the Klystron equation in z-coordinate.

$$\dot{z}_1 = -a_1 z_1 + a_1 cos(z_2) u_1 + a_1 sin(z_2) u_2 \tag{29}$$

$$\dot{z}_2 = -a_1 \frac{sin(z_2)}{z_1} u_1 + a_1 \frac{cos(z_2)}{z_1} u_2. \tag{30}$$

and

$$y_1^k = \sum_{i=1}^{N} c_i e^{-f_i w(t) z_1} \tag{31}$$

$$y_2^k = \sum_{i=1}^{N} d_i e^{-f_i w(t) z_1} + z_2 + 3 \cdot \frac{\pi}{180} \cdot R(t) \tag{32}$$

where

$$w(t) = M(0.01R(t) + 1)^{1.25}$$

$$M = \frac{K_g}{10\sqrt{KP_m}}.$$

Define

$$\overline{z}_1 = (0.01R(t) + 1)^{1.25} z_1 \tag{33}$$

$$\overline{z}_2 = z_2 + 3 \cdot \frac{\pi}{180} \cdot R(t). \tag{34}$$

The Klystron is expressed in $\overline{z}$-coordinate by

$$\dot{\overline{z}}_1 = -\overline{a}_1 \overline{z}_1 + b_{z11}(\overline{z}, R(t), \dot{R}(t)) u_1 + b_{z12}(\overline{z}, R(t), \dot{R}(t)) u_2 + E_{z1}(R(t), \dot{R}(t)) \tag{35}$$

$$\dot{\overline{z}}_2 = b_{z21}(\overline{z}, R(t), \dot{R}(t))u_1 + b_{z22}(\overline{z}, R(t), \dot{R}(t))u_2 + E_{z2}(R(t), \dot{R}(t)) \tag{36}$$

$$y_1^k = \sum_{i=1}^{N} c_i e^{-f_i M \overline{z}_1} \tag{37}$$

$$y_2^k = \sum_{i=1}^{N} d_i e^{-f_i M \overline{z}_1} + \overline{z}_2. \tag{38}$$

where

$$\begin{aligned}
&\overline{a}_1 = a_1 - 0.0125(0.01R(t)+1)^{-1}\dot{R}(t) \qquad (39)\\
&b_{z11}(\overline{z}, R(t), \dot{R}(t)) = a_1(0.01R(t)+1)^{1.25} cos(\overline{z}_2 - 3 \cdot \frac{\pi}{180} \cdot R(t)),\\
&b_{z12}(\overline{z}, R(t), \dot{R}(t)) = a_1(0.01R(t)+1)^{1.25} sin(\overline{z}_2 - 3 \cdot \frac{\pi}{180} \cdot R(t)),\\
&b_{z21}(\overline{z}, R(t), \dot{R}(t)) = -a_1 \frac{sin(\overline{z}_2 - 3 \cdot \frac{\pi}{180} \cdot R(t))}{\overline{z}_1},\\
&b_{z22}(\overline{z}, R(t), \dot{R}(t)) = a_1 \frac{cos(\overline{z}_2 - 3 \cdot \frac{\pi}{180} \cdot R(t))}{\overline{z}_1},\\
&E_{z1}(R(t), \dot{R}(t)) = 0,\\
&E_{z2}(R(t), \dot{R}(t)) = 3 \cdot \frac{\pi}{180}\dot{R}(t).
\end{aligned}$$

Note that $\overline{B}_z(\overline{z}, R(t), \dot{R}(t))$ is invertible for any nonzero $\overline{z}_1$. In $\overline{z}$-coordinate, state equations are dependent upon the ripple $R(t)$ but the output equations are independent upon the ripple $R(t)$.

Define

$$\overline{A}_z(R(t), \dot{R}(t)) = \begin{bmatrix} -\overline{a}_1 & 0 \\ 0 & 0 \end{bmatrix}, \tag{40}$$

$$\overline{z} = \begin{bmatrix} \overline{z}_1 \\ \overline{z}_2 \end{bmatrix}, \qquad u_z = \begin{bmatrix} u_1 \\ u_2 \end{bmatrix}, \tag{41}$$

$$E_z(R(t), \dot{R}(t)) = \begin{bmatrix} 0 \\ 3 \cdot \frac{\pi}{180}\dot{R}(t) \end{bmatrix}, \tag{42}$$

and

$$\overline{B}_z(\overline{z}, R(t), \dot{R}(t)) = \begin{bmatrix} b_{z11}(\overline{z}, R(t), \dot{R}(t)) & b_{z12}(\overline{z}, R(t), \dot{R}(t)) \\ b_{z21}(\overline{z}, R(t), \dot{R}(t)) & b_{z22}(\overline{z}, R(t), \dot{R}(t)) \end{bmatrix}. \tag{43}$$

Then, (39) and (40) are represented by

$$\dot{\overline{z}} = \overline{A}_z(R(t), \dot{R}(t))\overline{z} + \overline{B}_z(\overline{z}, R(t), \dot{R}(t))u_z + E_z(R(t), \dot{R}(t)). \tag{44}$$

# 3 The RF cavity

Figure 3 shows the RF cavity model.

RF cavity has four inputs, HPRF_I, HPRF_Q, BEAM_I, and BEAM_Q, two outputs, CAV_FLD_I and CAV_FLD_Q.

Let $u_1^c$=HPRF_I, $u_2^c$=HPRF_Q, $u_3^c$=BEAM_I, $u_4^c$=BEAM_Q and let $y_1^c$=CAV_FLD_I, $y_2^c$=CAV_FLD_Q. Then, the RF cavity can be expressed in the state space form.

$$\dot{x} = Ax + Bu^c \tag{45}$$

$$y^c = Cx \tag{46}$$

where

$$A = \begin{bmatrix} a-\frac{1}{50}c_1 & b-\frac{1}{50}c_2 & 0 & 0 & 0 & 0 & \frac{1}{50}c_3 & \frac{1}{50}c_4 \\ 1 & 0 & 0 & 0 & 0 & 0 & 0 & 0 \\ -\frac{1}{50}c_1 & -\frac{1}{50}c_2 & a & b & 0 & 0 & \frac{1}{50}c_3 & \frac{1}{50}c_4 \\ 0 & 0 & 1 & 0 & 0 & 0 & 0 & 0 \\ 0 & 0 & -\frac{1}{50}c_3 & -\frac{1}{50}c_4 & a-\frac{1}{50}c_1 & b-\frac{1}{50}c_2 & 0 & 0 \\ 0 & 0 & 0 & 0 & 1 & 0 & 0 & 0 \\ 0 & 0 & -\frac{1}{50}c_3 & -\frac{1}{50}c_4 & -\frac{1}{50}c_1 & -\frac{1}{50}c_2 & a & b \\ 0 & 0 & 0 & 0 & 0 & 0 & 1 & 0 \end{bmatrix},$$

$$B = \begin{bmatrix} \frac{2}{50} & 0 & -2eta & 0 \\ 0 & 0 & 0 & 0 \\ \frac{2}{50} & 0 & -2eta & 0 \\ 0 & 0 & 0 & 0 \\ 0 & \frac{2}{50} & 0 & -2eta \\ 0 & 0 & 0 & 0 \\ 0 & \frac{2}{50} & 0 & -2eta \\ 0 & 0 & 0 & 0 \end{bmatrix},$$

$$C = \begin{bmatrix} c_1 & c_2 & 0 & 0 & 0 & 0 & -c_3 & -c_4 \\ 0 & 0 & c_3 & c_4 & c_1 & c_2 & 0 & 0 \end{bmatrix}$$

$$a = -\frac{2}{\tau}$$

$$b = -(\frac{1}{\tau^2} + KDW^2)$$

$$c_1 = \frac{KR}{\tau}$$

$$c_2 = \frac{KR}{\tau}(\frac{1}{\tau} - \frac{KDW}{2KQo})$$
$$c_3 = \frac{KR}{2\tau \cdot KQo}$$
$$c_4 = \frac{KR}{2\tau KQo}(\frac{1}{\tau} + 2KDW \cdot KQo).$$

Parameters of RF cavity are given in [6].

Also, FLD_I and FLD_Q of the cavity Field Sample System are given by

$$FLD\_I = FA \cdot cos(GD) \cdot y_1^c - FA \cdot sin(GD) \cdot y_2^c \tag{47}$$
$$FLD\_Q = FA \cdot sin(GD) \cdot y_1^c + FA \cdot cos(GD) \cdot y_2^c \tag{48}$$

and FLD_AMP and FLD_PHS of the cavity Field Sample System are given by

$$FLD\_AMP = \sqrt{FLD\_I^2 + FLD\_Q^2}$$
$$FLD\_PHS = tan^{-1}(\frac{FLD\_Q}{FLD\_I})$$

where

$$FA = 0.00037809$$
$$GD = \frac{\pi}{180} \cdot (-0.039455).$$

The RF cavity as given in (45), (46) is Hurwitz stable and is inverse stable as well.

# 4 RIPPLE Estimation

The purpose of the low level RF control(LLRF) system is to maintain the field stability within $\pm 1.0\%$ amplitude and $1.0^\circ$ phase. The present LLRF control system is based on PID control scheme[4],[5],[6]. As has been investigated in [3],[7], the high voltage power supply ripple has influence on the LLRF PID control system. Low frequency ripple does not deteriorate the performance of the closed loop system seriously but high frequency ripple deteriorates the performance of the closed loop system seriously.

For the remedy to the poor performance of the PID controlled LLRF control system due to the high frequency high voltage power supply ripple, we propose a feedforward control of the estimate of the ripple. The feedforward improves the performance significantly[1].

In this section, we address the ripple estimator which estimates the ripple $R(t)$ and its time derivative $\frac{dR(t)}{dt}$.

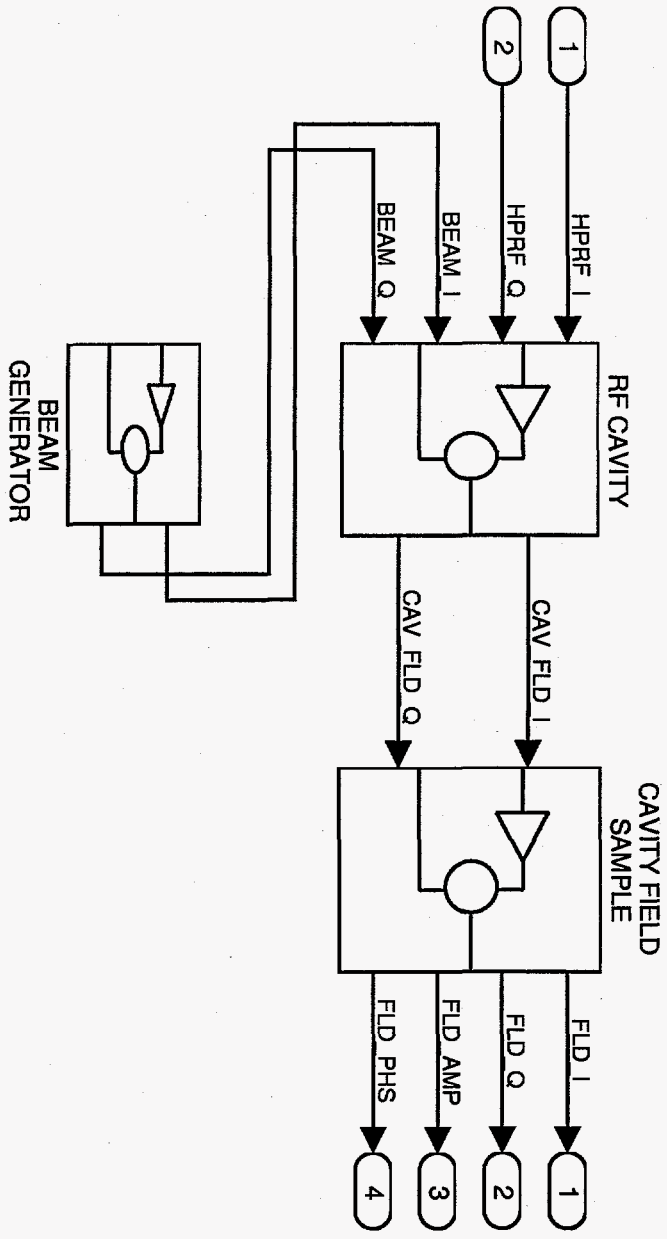


Figure 3: A RF cavity Model and a cavity Field Sample System

We first consider equations as given in (21) and (22).

$$z_1 = \sqrt{x_1^2 + x_2^2} \tag{49}$$

$$z_2 = tan^{-1}(\frac{x_2}{x_1}) \tag{50}$$

where $x_1$ and $x_2$ satisfy

$$\dot{x}_1 = -a_1 x_1 + a_1 u_1 \tag{51}$$

$$\dot{x}_2 = -a_1 x_2 + a_1 u_2 \tag{52}$$

and $u_1$=LLRF_I, $u_2$=LLRF_Q. Given LLRF_I and LLRF_Q, we can obtain $z_1$ and $z_2$ by solving differential equations (51), (52) and algebraic equations (45), (46).

Second, we consider equations given by (19) and (20).

$$HPRF\_I = 10\sqrt{KP_m} \cdot y_1^k \cdot cos(y_2^k) \tag{53}$$

$$HPRF\_Q = 10\sqrt{KP_m} \cdot y_1^k \cdot sin(y_2^k). \tag{54}$$

From (53) and (54), for given HPRF_I and HPRF_Q, we obtain the normalized amplitude $y_1^k$ and the normalized phase $y_2^k$ of the klystron by solving algebraic equations.

$$y_1^k = \frac{1}{10\sqrt{KP_m}}\sqrt{HPRF\_I^2 + HPRF\_Q^2} \tag{55}$$

$$y_2^k = tan^{-1}(\frac{HPRF\_Q}{HPRF\_I}). \tag{56}$$

Third, we consider the klystron model as given in Figure 1. In Figure 1, the normalized amplitude of the klystron is the output of the look-up table **AMPLITUDE SATURATION**. The input of the look-up table **AMPLITUDE SATURATION** is given by

$$A = \frac{K_g}{10\sqrt{KP_m}}(0.01R(t) + 1)^{1.25} \cdot z_1 \tag{57}$$

in $z$-coordinate, or

$$A = \frac{K_g}{10\sqrt{KP_m}}\overline{z}_1 \tag{58}$$

in $\overline{z}$-coordinate. Also, there exists a region of $(A, y_1^k)$ pairs where there is an inverse look-up table of the look-up table **AMPLITUDE SATURATION**. This region can be extracted from data given in Table 1 and Table 2. As in the case of **AMPLITUDE SATURATION**, we obtain the curve fitting equation for the inverse look-up table for **AMPLITUDE SATURATION**. Since, in controller design, we make use of the output equations (31) and (32)

or (37) and (38) which are based on the curve fitting equation, in order to obtain the curve fitting equation for the inverse look-up table for **AMPLITUDE SATURATION** within the region of invertibility, we use the output equation as given in (37). Based on the generated data pairs from (37) where the selected data of $y_1^k$ and $\overline{z}_1$ guarantee invertibility, we obtain the curve fitting equation as follows.

$$\overline{z}_1 = \sum_{i=1}^{N} c_i^z e^{-f_i^z y_1^k} \tag{59}$$

where $N = 7$, coefficients $f_i^z$, $i = 1, 2, \cdots, N$ are given and the coefficients $c_i^z$, $i = 1, 2, \cdots, N$ are obtained by applying the optimization toolbox of Matlab/Simulink. Table 5 gives the data of the coefficients of the curve fitting. The nonlinear least square algorithm in Matlab/Simulink guarantees 1% accuracy of the curve fitting.

| | | | |
|---|---|---|---|
| $f_1^z$ | 0.50 | $c_1^z$ | 246379.701273592 |
| $f_2^z$ | 0.75 | $c_2^z$ | -1633291.85956396 |
| $f_3^z$ | 1.00 | $c_3^z$ | 4505197.57531207 |
| $f_4^z$ | 1.25 | $c_4^z$ | -6618176.95439792 |
| $f_5^z$ | 1.50 | $c_5^z$ | 5460679.73050349 |
| $f_6^z$ | 1.75 | $c_6^z$ | -2399431.11098975 |
| $f_7^z$ | 2.00 | $c_7^z$ | 438643.015066461 |

Table 5. Coefficients of Curve fitting equation for Inverse **AMPLITUDE SATURATION**

The estimate of the ripple $R(t)$ and the estimate of the time derivative $\frac{dR(t)}{dt}$ of the ripple $R(t)$ are obtained by considering the klystron system both in $z$-coordinate and $\overline{z}$-coordinate. The relation between $z$-coordinate and $\overline{z}$-coordinate is given by

$$\overline{z}_1 = (0.01R(t) + 1)^{1.25} z_1 \tag{60}$$

$$\overline{z}_2 = z_2 + 3 \cdot \frac{\pi}{180} \cdot R(t). \tag{61}$$

Whenever $x_1$ and $x_2$ are obtained from (51) and (52), then we can obtain $z_1$ by using (49) and (50), and also whenever $y_1^k$ is obtained from (55), we can obtain $\overline{z}_1$ by using (59). For

given $z_1$ and $\overline{z}_1$, we can obtain the estimate $\hat{R}(t)$ of the ripple $R(t)$ by solving algebraic equation (60).

$$\hat{R}(t) = 100((\frac{\overline{z}_1(t)}{z_1(t)})^{0.8} - 1.0). \tag{62}$$

Also, the estimate $\dot{\hat{R}}(t)$ of time derivative $\dot{R}(t)$ of the ripple $R(t)$ is obtained by differentiation of $\hat{R}(t)$.

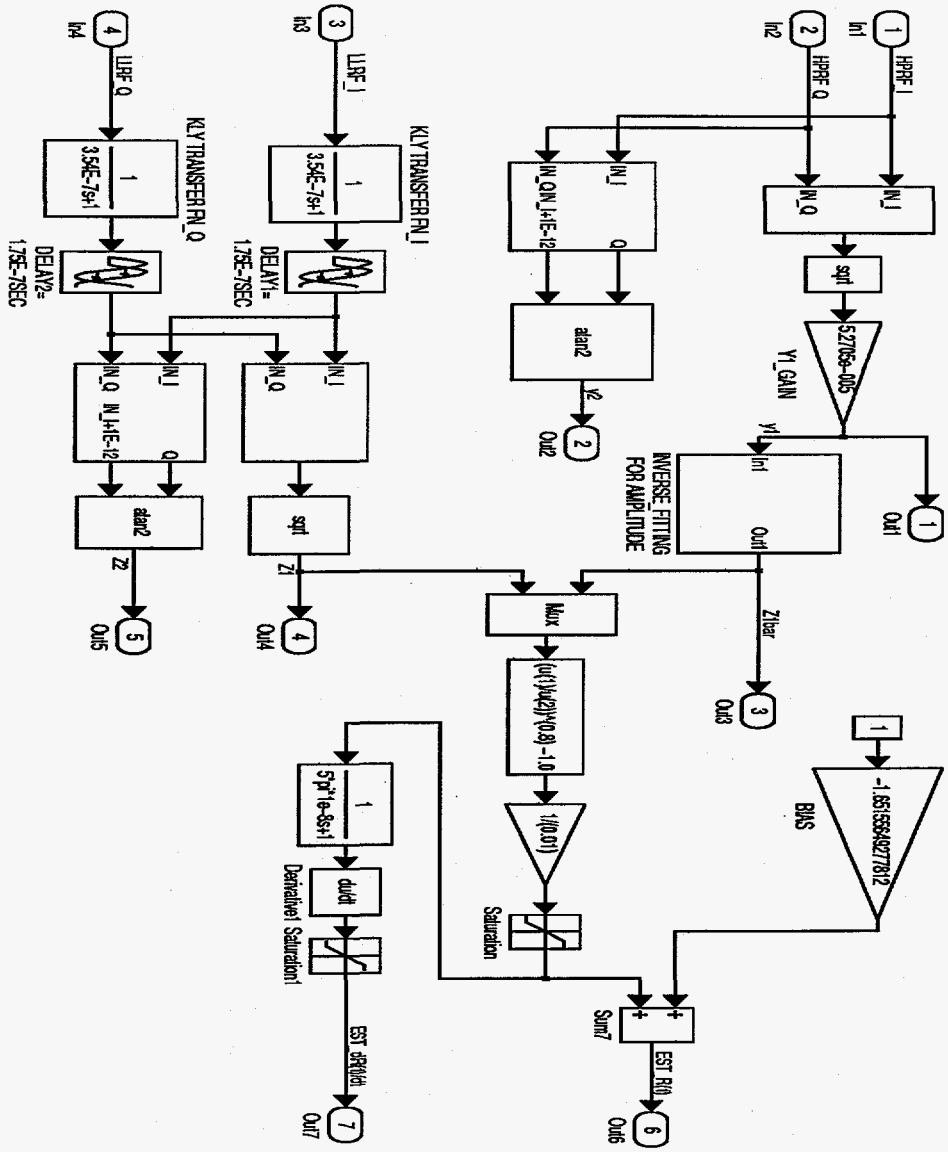


Figure 4: The ripple estimator

# 5 Feedforward Control of the estimate $\hat{R}(t)$

The work in [7] shows that the **AMPLITUDE DEPENDENCE** of the high voltage power supply ripple is not seriously effective to the performance of tracking set points of the LLRF control system. The main effect of the high voltage power supply ripple is due to **PHASE DEPENDENCE**.

In this section, we propose a feedforward control of the estimate $\hat{R}(t)$. The feedforward control improves the tracking performance of the field phase significantly.

We consider the output equations as given in (27), (28) and (55), (56).

$$y_1^k = \sum_{i=1}^{N} c_i e^{-f_i w(t) z_1} \tag{63}$$

$$y_2^k = \sum_{i=1}^{N} d_i e^{-f_i w(t) z_1} + z_2 + 3 \cdot \frac{\pi}{180} \cdot R(t) \tag{64}$$

$$y_1^k = \frac{1}{10\sqrt{KP_m}} \sqrt{HPRF\_I^2 + HPRF\_Q^2} \tag{65}$$

$$y_2^k = tan^{-1}(\frac{HPRF\_Q}{HPRF\_I}) \tag{66}$$

where

$$w(t) = M(0.01R(t) + 1)^{1.25}.$$

Also, the amplitude and the phase of the high power RF(HPRF) amplifier are

$$HPRF\_AMP = \sqrt{HPRF\_I^2 + HPRF\_Q^2} \tag{67}$$

$$HPRF\_PHS = tan^{-1}(\frac{HPRF\_Q}{HPRF\_I}). \tag{68}$$

In (64), the normalized phase $y_2^k$ is affected by the **PHASE DEPENDENCE** term

$$3 \cdot \frac{\pi}{180} \cdot R(t). \tag{69}$$

When $R(t)$ is estimated within a satisfactory accuracy, a feedforward control loop from the estimate $\hat{R}(t)$ to $y_2^k(t)$ can attenuate the effect the high voltage power supply ripple $R(t)$ to the phase of the klystron and so the phase of field.

Define a feedforward loop gain from the estimate $\hat{R}(t)$ as

$$-3 \cdot \frac{\pi}{180} \tag{70}$$

and consider $\overline{HPRF\_AMP}$, $\overline{HPRF\_PHS}$ defined by

$$\overline{HPRF\_AMP} = HPRF\_AMP \tag{71}$$

$$\overline{HPRF\_PHS} = HPRF\_PHS - 3 \cdot \frac{\pi}{180} \cdot \hat{R}(t). \tag{72}$$

Plugging (68), (66), and (64) into (72), we obtain

$$\begin{aligned} \overline{HPRF\_PHS} &= y_2^k - 3 \cdot \frac{\pi}{180} \cdot \hat{R}(t) \\ &= \sum_{i=1}^{N} d_i e^{-f_i w(t) z_1} + z_2 + 3 \cdot \frac{\pi}{180} \cdot R(t) - 3 \cdot \frac{\pi}{180} \cdot \hat{R}(t) \\ &= \sum_{i=1}^{N} d_i e^{-f_i w(t) z_1} + z_2 + 3 \cdot \frac{\pi}{180} (R(t) - \hat{R}(t)). \end{aligned} \tag{73}$$

If there exists a bounded function $\epsilon(t) < 1.0$ such that

$$|\frac{\hat{R}(t)}{R(t)}| \leq \epsilon(t), \quad \forall t \geq t_0,$$

then, we can attenuate the effect of the high voltage power supply ripple $R(t)$ to the phase of the field. The estimate $\hat{R}(t)$ as given in (62) is defined by the solution of an algebraic equation (60). $z_1$ is given by (49) whose variables are the state of the exactly same system of **FILTER AND AMPLIFIER** of a klystron. $\overline{z}_1$ is given by the curve fitting equation (59) of the lookup table of inverse **AMPLITUDE SATURATION**. The accuracy of the estimate $\hat{R}(t)$ is determined by the curve fitting equation (59). The nonlinear least square algorithm used for the curve fitting guarantees 1% accuracy.

Of course, we have to consider the **AMPLITUDE DEPENDENCE** represented by $(0.01R(t) + 1)^{1.25}$(1%ripple). However, this amount does not have an influence on the phase of the field significantly[3],[7].

From (71) and (72), we reconstruct M_HPRF_I and M_HPRF_Q which drive the RF cavity.

$$M\_HPRF\_I = \overline{HPRF\_AMP} \cdot cos(\overline{HPRF\_PHS}) \tag{74}$$

$$M\_HPRF\_Q = \overline{HPRF\_AMP} \cdot sin(\overline{HPRF\_PHS}). \tag{75}$$

Figure 5 shows the feedforward loop of the estimate $\hat{R}(t)$.

Figure 6 shows the LLRF control system including PID controller, the ripple estimator and the feedforward loop of the estimate $\hat{R}(t)$.

Figure 7 through Figure 10 show the simulation results of the proposed LLRF Control System with adaptive feedforward of the estimate $\hat{R}(t)$. The ripple is

$$R(t) = sin(2\pi ft), \quad f = 40kHz.$$

The peak-to-peak amplitude error is 0.864% and the peak-to-peak phase error at steady state is 0.0474°. As shown in Figure 9, the phase error of the field is greatly reduced(438% improvement).

In order to compare the performance, we also simulate the closed loop system without the feedforward of the estimate $\hat{R}(t)$. Figure 11 and Figure 12 show the results. The peak-to-peak amplitude error is 0.922% and the peak-to-peak phase error at steady state is 2.0752°.

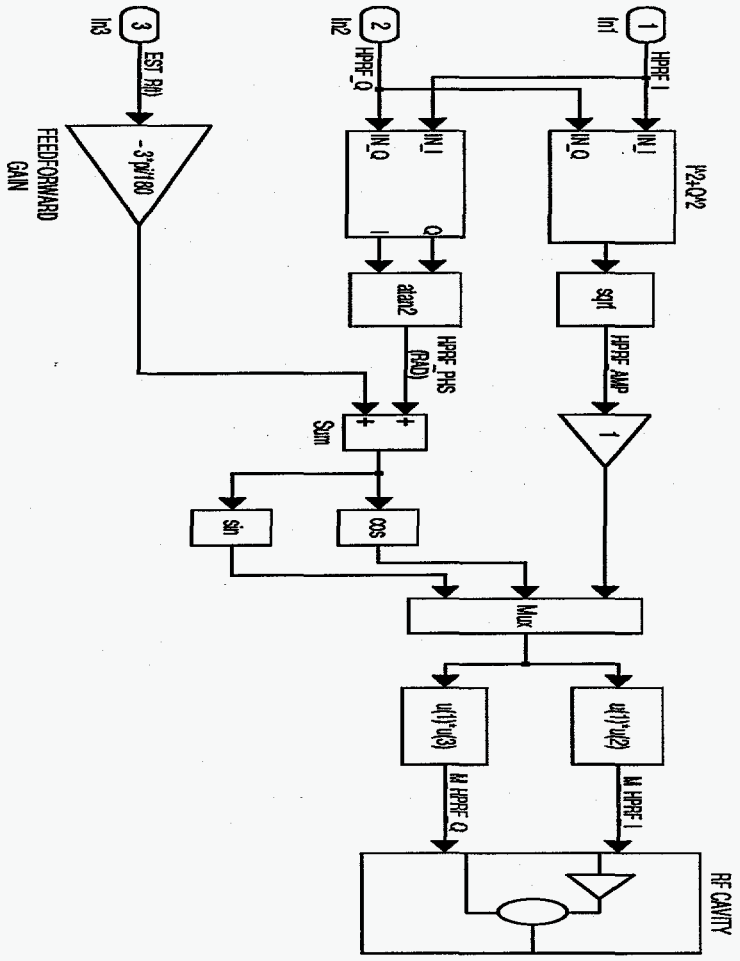


Figure 5: The Adaptive Feedforward of the Estimate $\hat{R}(t)$

# References


[1] K. J. Astrom and T. Hagglund, *PID controllers:theory, design, and tuning*, Second Edition, Instrument Society of America, Research Triangle Park, NC, 1995.

[2] C.T. Chen, *Introduction to linear System Theory*, Second edition, Rinehart and Winston, New York, 1986.

[3] Sung-il Kwon, " 0.3% high voltage power supply ripple response test," *preprint.*

[4] D. Rees, J. Bradley III, K. Cummings, M. Lynch, A. Regan, T. Rohlev, W. Roybal, Y.M. Wang, "Design and test results of the low energy demonstration accelerator(LEDA) RF systems," *presented in XIX International LINAC Conference*, Chicago, USA, 1998.

[5] A. Regan and C. Ziomek, "APT LLRF control system model results," *presented in XIX International LINAC Conference*, Chicago, USA, 1998.

[6] Chris Ziomek and Amy Regan, "Simplification of Matrixx Model: Preliminary LLRF System Design," *Technical Note*, AOT-5-TN:001, RF Technology Group, AOT Division, Los Alamos National Laboratory, 1996.

[7] Chris Ziomek and Amy Regan, "Superconducting system model; HVPS ripple model," *Technical Note*, AOT-5-TN:003, RF Technology Group, AOT Division, Los Alamos National Laboratory, 1996.

[8] Chris Ziomek and Amy Regan, "Model Multiple Klystrons, Pulsed Beam (SC and NC)," *Technical Note*, AOT-5-TN:005, RF Technology Group, AOT Division, Los Alamos National Laboratory, 1996.

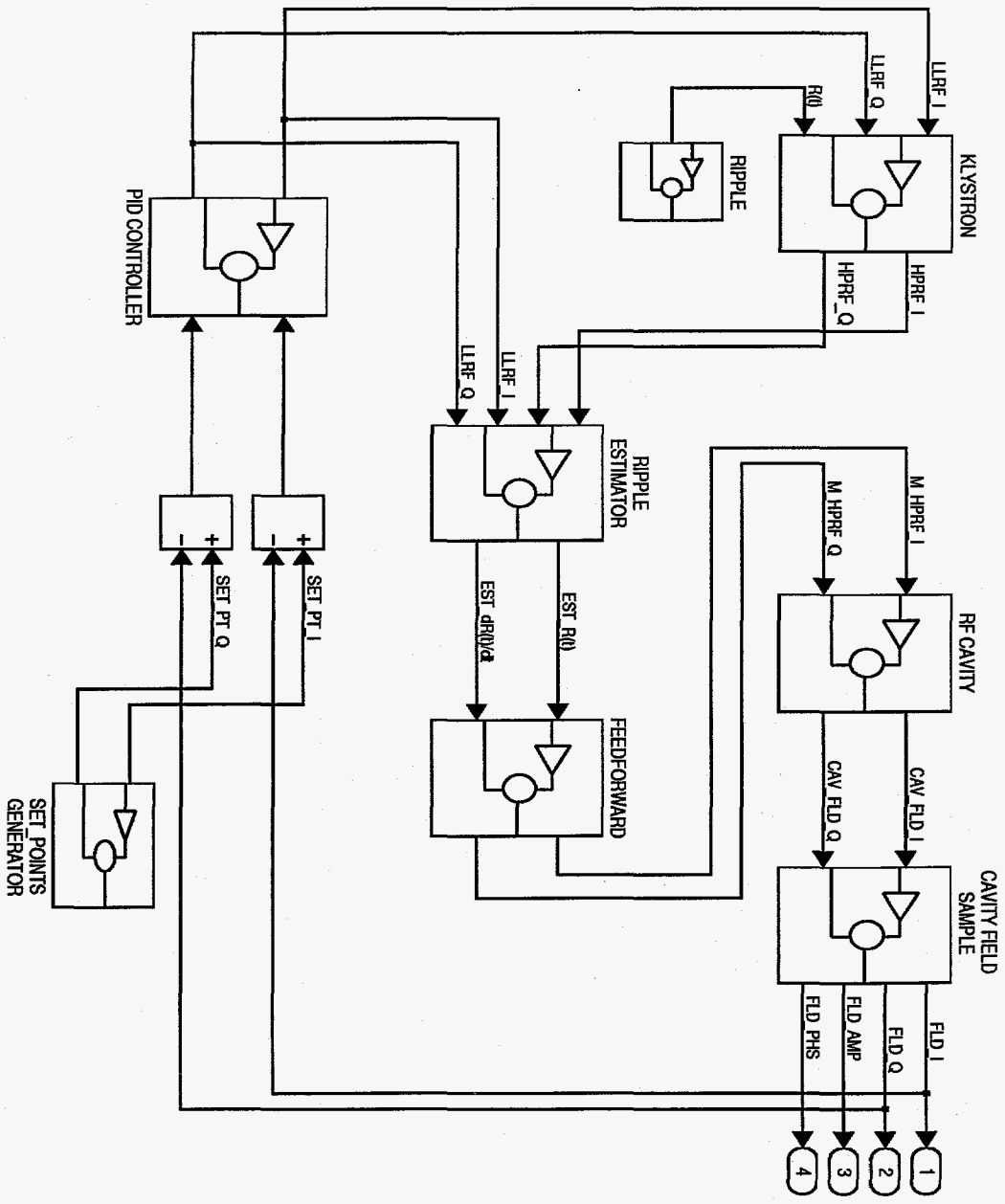


Figure 6: The LLRF Control System with Adaptive Feedforward of the Estimate $\hat{R}(t)$

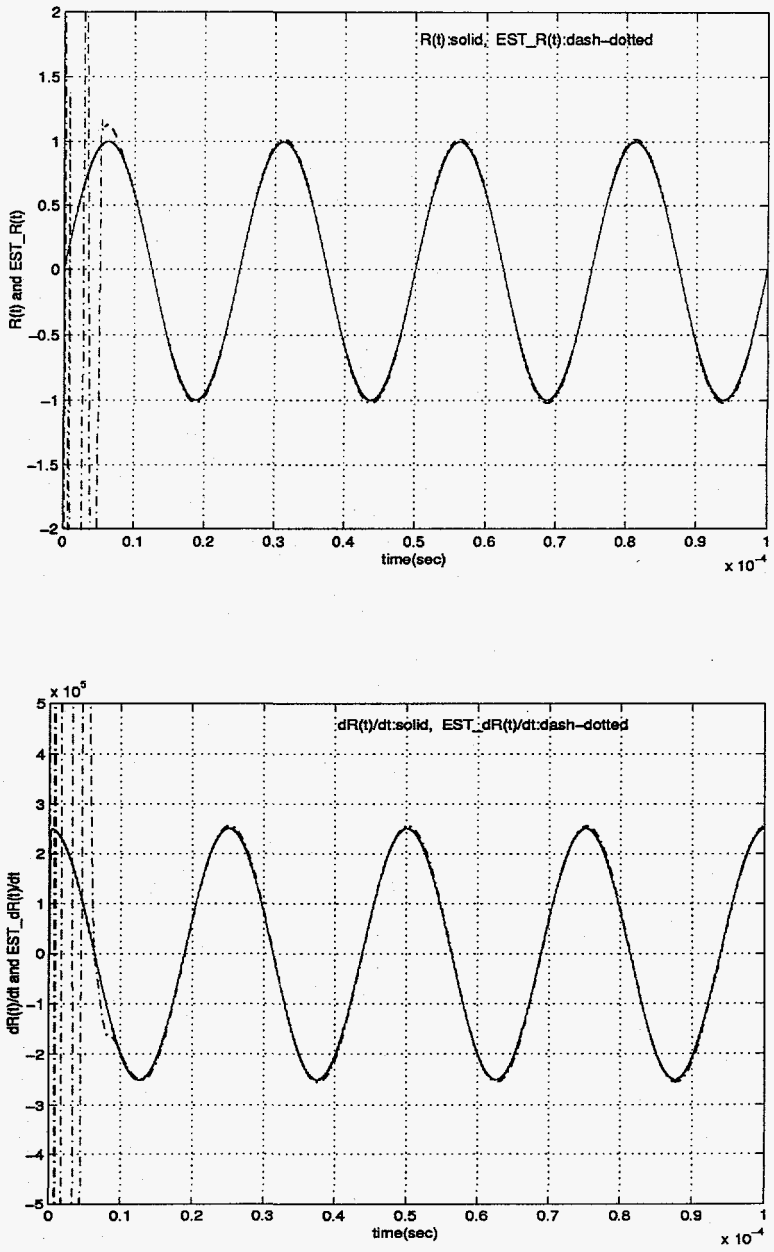


Figure 7: Ripple $R(t)$ and its time derivative $dR(t)/dt$ and their estimates $EST\_R(t)$ and $EST\_dR(t)/dt$

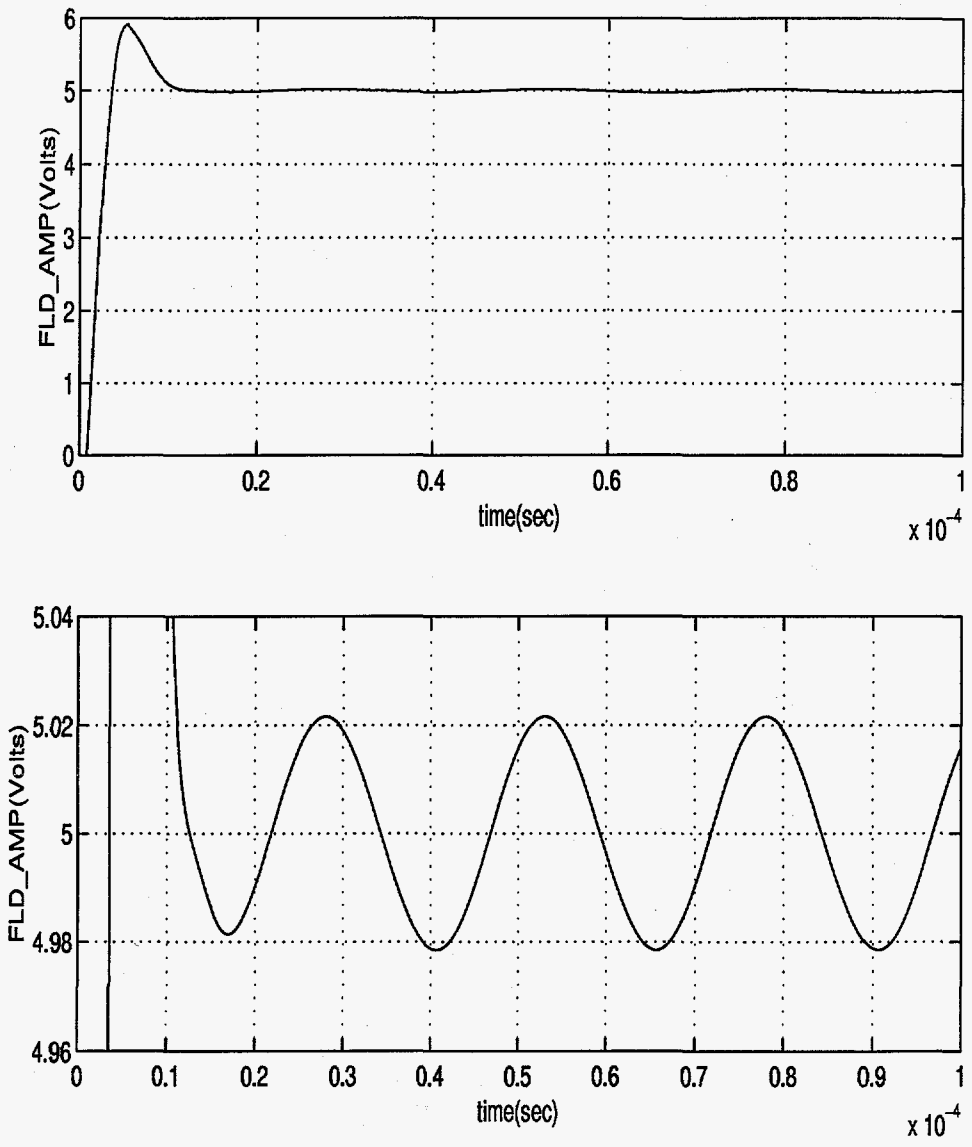


Figure 8: Amplitude of Field, FLD_AMP with feedforward control of the Estimate $\hat{R}(t)$

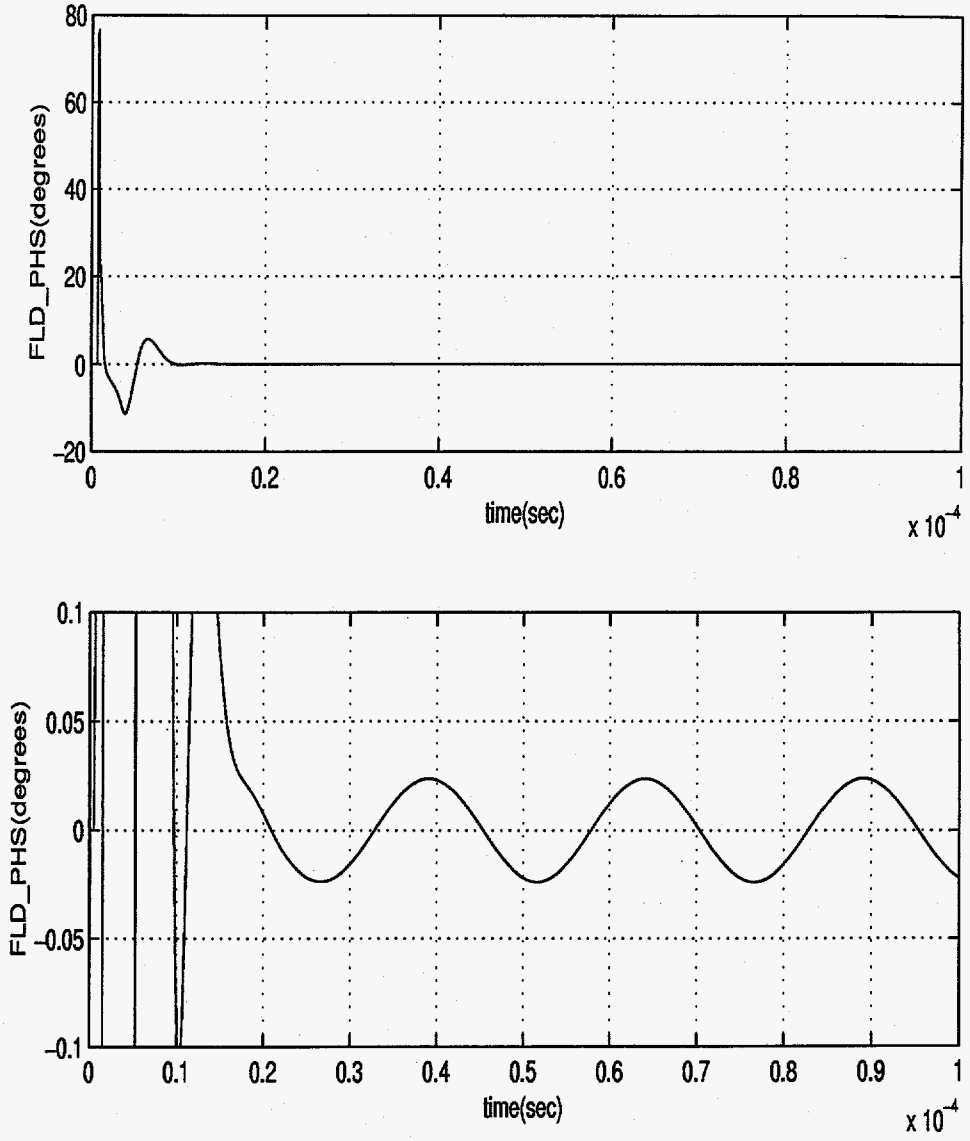


Figure 9: Phase of Field, FLD_PHS with feedforward control of the Estimate $\hat{R}(t)$

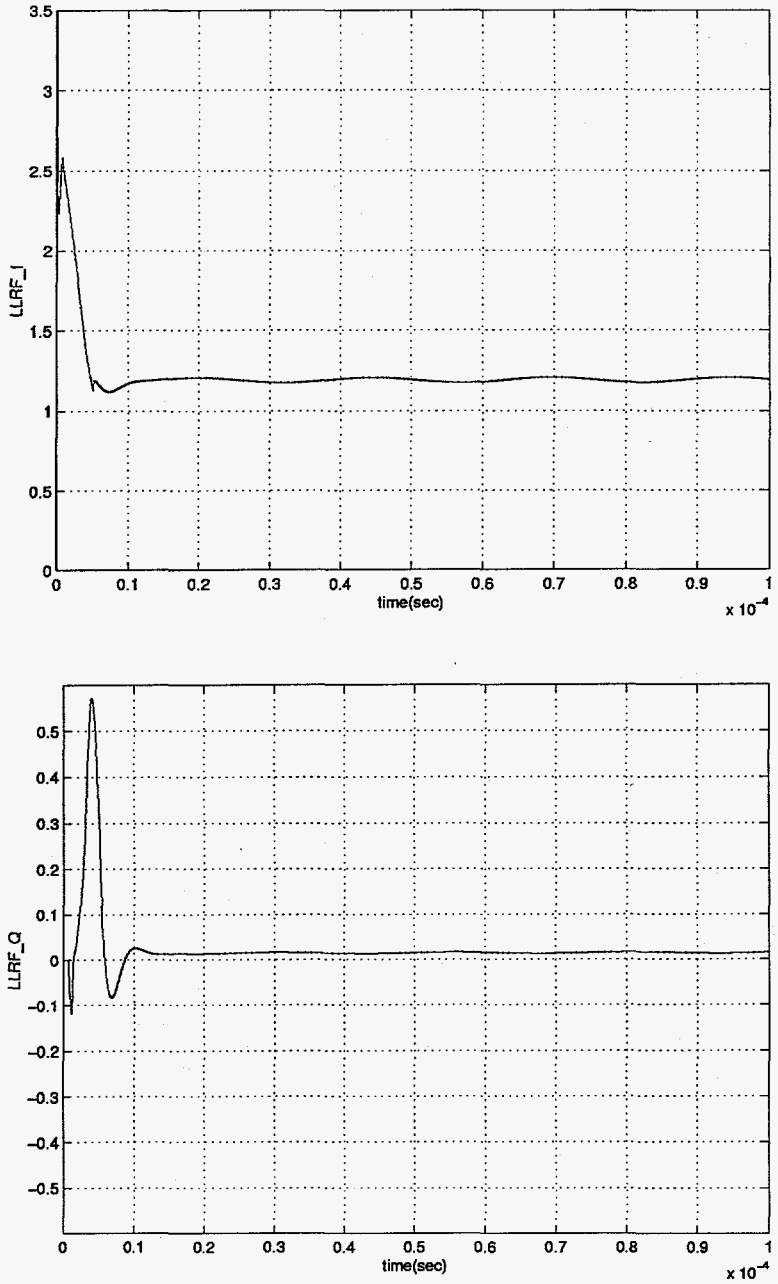


Figure 10: LLRF_I and LLRF_Q with feedforward control of the Estimate $\hat{R}(t)$

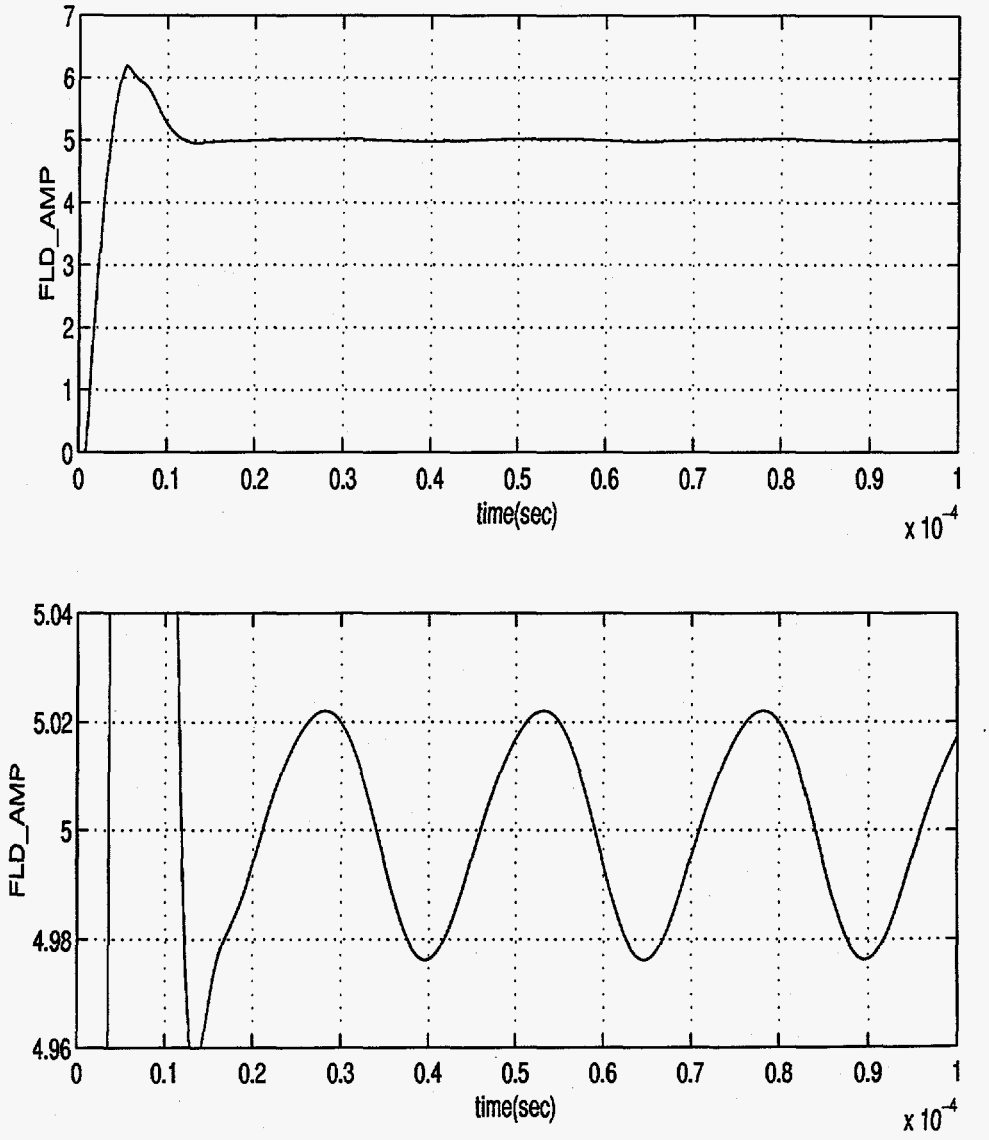


Figure 11: Amplitude of Field, FLD_AMP without feedforward control

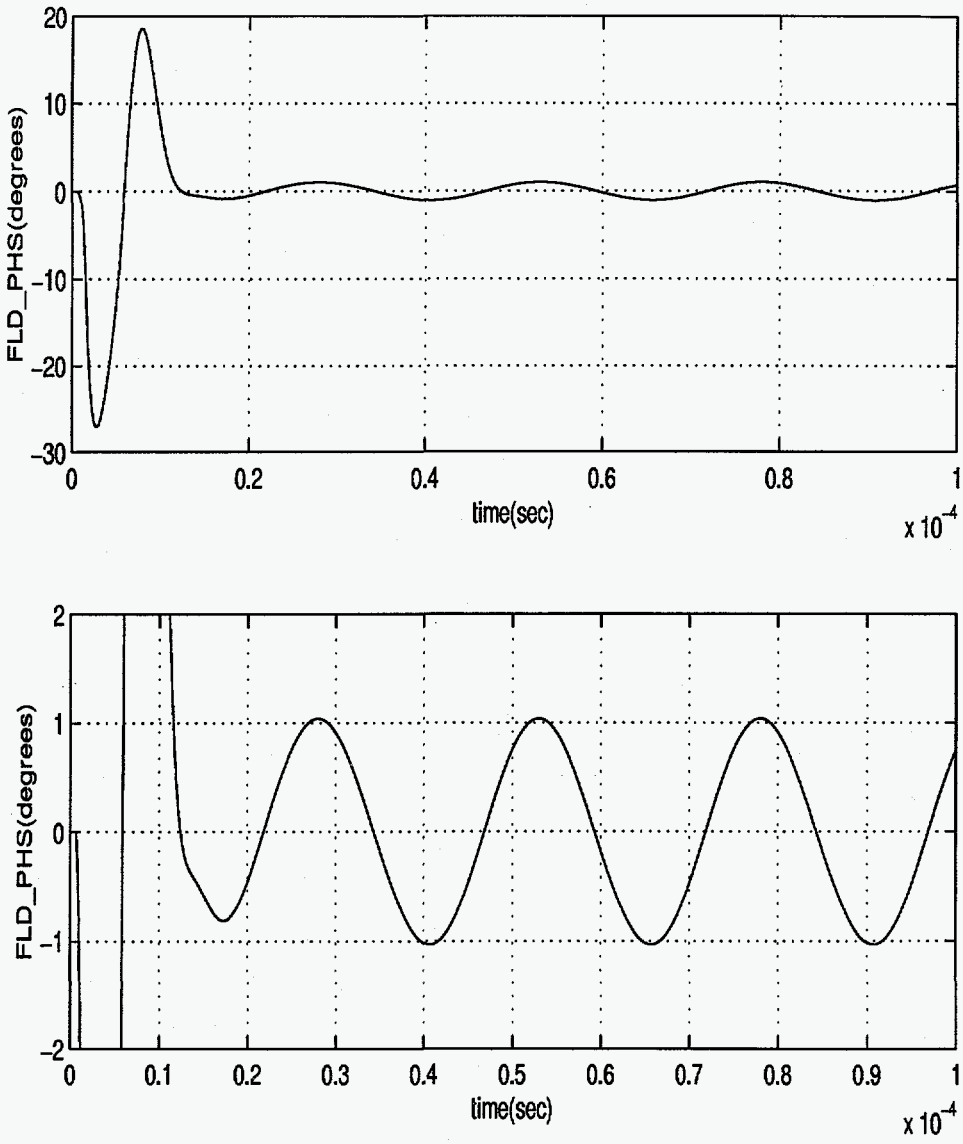


Figure 12: Phase of Field, FLD_PHS without feedforward control